Emission in the Biological Window from AIE-Based Carbazole-Substituted Furan-Based Compounds for Organic Light-Emitting Diodes and Random Lasers

Kamila Lupinska, Sonia Kotowicz, Anna Grabarz, Mariola Siwy, Karolina Sulowska, Sebastian Mackowski, Lulu Bu, Yann Bretonnière, Chantal Andraud, Ewa Schab-Balcerzak, et al.

ACS OMEGA

Open Access

http://pubs.acs.org/journal/acsodf

Article

Emission in the Biological Window from AIE-Based Carbazole-Substituted Furan-Based Compounds for Organic Light-Emitting Diodes and Random Lasers

Kamila Lupinska,* Sonia Kotowicz, Anna Grabarz, Mariola Siwy, Karolina Sulowska, Sebastian Mackowski, Lulu Bu, Yann Bretonnière, Chantal Andraud, Ewa Schab-Balcerzak, and Lech Sznitko*

Cite This: *ACS Omega* 2024, 9, 40769−40782

Read Online

ACCESS | Metrics & More | Article Recommendations | Supporting Information

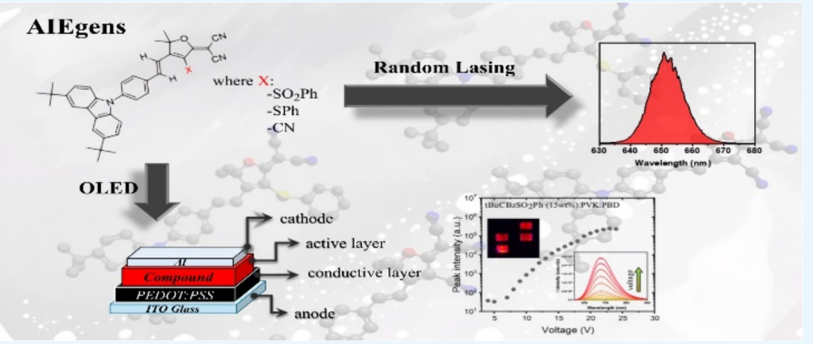

ABSTRACT: The emission quenching observed in devices utilizing luminescent materials such as solid thin films is a prevalent issue. Consequently, searching for new organic luminescent compounds exhibiting aggregation-induced emission (AIE) behavior and characterized by relatively simple and cost-effective synthesis is of crucial interest among applications from optoelectronics and organic lasing branches. Herein, we report the optical properties of three furan-based carbazole-substituted compounds, namely, tBuCBzSO$_2$Ph, tBuCBzSPh, and tBuCbzTCF, exhibiting the aforementioned AIE phenomenon. The optical properties of dyes were determined in classical spectroscopic experiments supported by quantum-chemical calculations. The thermal investigations and electrochemical properties of dyes were performed to verify their usefulness in the construction of organic light-emitting diodes (OLEDs). In pursuit of this objective, OLEDs with a different design were fabricated, and their performance was subject to evaluation. In more detail, the different design strategies relying on the utilization of neat-dye films, as well as the preparation of dye-doped poly(9-vinylcarbazole):2-(4-*tert*-butylphenyl)-5-(4-biphenylyl)-1,3,4-oxadiazole (PVK:PBD) matrices were examined. The analysis that was conducted indicated the superior potential of tBuCBzSPh for optoelectronic applications. Notably, the positive impact of the AIE effect on the emission of the OLEDs and the ability to establish the lasing phenomenon in asymmetric, poly(methyl methacrylate) (PMMA)-doped polymeric slab waveguides were verified. The study showed that the combination of the strong intramolecular charge transfer (ICT) effect with dye aggregation enables the tuning of the emission of the OLED toward the first biological window, making examined dyes promising candidates for biomedical purposes. The same optical region can be attained for laser emission at relatively low pumping conditions, reaching as low as 7.3 kW of optical power for the tBuCBzSO$_2$Ph compound.

INTRODUCTION

In the past few years, small organic compounds emitting in the near-infrared (NIR) region of the radiation have gained attention from various fields of research. In this scope, considerable efforts have been made to explore new implementations of these compounds. Especially organic light-emitting diodes (OLEDs) and random lasers (RL) are particularly interesting to scientists because of their potential use in biological applications as light sources with excellent biocompatibility and flexibility.[1,2] For instance, OLED technology can be adapted in biomedicine for lab-on-chip,[3,4] optogenetic,[5,6] therapeutic treatment,[7,8] and health monitoring or biosensor applications.[9−11] On the other hand, the

Received: June 12, 2024
Revised: September 5, 2024
Accepted: September 10, 2024
Published: September 18, 2024

implementation of RL in the biomedical field is also well-known and commonly used.[12−14] Besides, an additional advantage arising from both of these kinds of light-emitting devices is the uncomplicated fabrication process and low production cost.[15]

Among the various techniques used to fabricate high-performance electronic devices, one relies on the utilization of organic compounds containing carbazole units in the structure.[16−19] The aforementioned class of dyes demonstrates good thermal stability, high triplet energy, and efficient hole transport, which are all reported to have desirable properties.[20] Consequently, molecules containing the carbazole group are widely utilized for fabricating OLEDs,[21,22] organic field effect transistors (OFETs),[23,24] and organic−inorganic hybrid perovskite solar cells (PSCs).[25,26]

OLED development mainly depends on the fabrication and functionalization of thin polymer films, which are used as the active matrix in the devices.[27−29] Additionally, it should be emphasized that polymer thin films play a crucial role in achieving and enhancing laser emission.[30] Unfortunately, many dyes showing excellent emission properties in a solvent medium experience severe emission quenching during aggregation (aggregation-induced quenching − ACQ).[31] As a result of this detrimental effect, they can no longer be used as high-performance light-emitting organic devices. Consequently, luminescence quenching in aggregate states significantly restricts the progress of the OLED's implementation. In this context, using aggregation-induced emission (AIE) compounds as active layers in organic optoelectronic materials represents an original and practical method to overcome these limitations.[32] In the past, it has been demonstrated that the AIE phenomenon can have a positive impact on emission efficiency in OLED devices[33] and low-efficiency roll-off.[34] In particular, blue AIE-gens have been investigated and successfully applied in a two-color hybrid white OLED.[34] The ACQ effect has also limited the growth of high-laser-gain materials and their development due to reduced luminescence efficiency and lower optical gain, resulting in difficulty in achieving efficient lasing. On the other hand, we recently have shown that AIE can positively impact laser light enhancement and can decrease the threshold of laser action.[35]

Despite the numerous advantages of OLEDs, it is worth adding that RL also garners great interest among different emitters. Nowadays, issues correlated with the external cavity occurring in various lasers lead to limitations of their application. RLs, on the other hand, rely on the scattering centers inside the sample, allowing optical feedback and thus obtaining laser action. From this point of view, compounds capable of random lasing (RLng) are promising materials in optical sensors,[36] light therapy,[37] display technologies,[38] nanofiber-based photonic devices[39] or in medicine, for cancer diagnostic applications.[40]

Different strategies to fabricate OLED devices and materials exhibiting RLng phenomena involve employing dyes containing two different groups with opposite functions in the molecules (i.e., electron-donating and withdrawing moieties), which can induce an intermolecular charge transfer (ICT) process.[41] This effect can be promoted when both mentioned groups are connected by a bridge rich in π-electrons, enabling charge conductivity.[41] In addition, the rapid deactivation of the excited molecule that occurs in ICT molecules has also been exploited in laser applications.[42] Thus, small organic compounds with a donor-π−acceptor (D-π−A) design are highly desirable in electrochemical and laser applications.[43−47]

Herein, we focused on three compounds: tBuCBzSO$_2$Ph (2-[4-[(1E)-2-[4-(3,6-Di*tert*-butyl-9H-carbazol-9-yl)phenyl]-ethenyl]-3-phenylsulfonyl-5,5-dimethyl-2(5H)-furanylidene]-propanedinitrile), tBuCBzSPh (2-[4-[(1E)-2-[4-(3,6-Di*tert*-butyl-9H-carbazol-9-yl)phenyl]-ethenyl]-3-phenylthio-5,5-dimethyl-2(5H)-furanylidene]-propanedinitrile), and tBuCBzTCF (2-[4-[(1E)-2-[4-(3,6-Di*tert*-butyl-9H-carbazol-9-yl)phenyl]-ethenyl]-3-cyano-5,5-dimethyl-2(5H)-furanylidene]-propanedinitrile) (see structures in Figure 1), containing carbazole units serving as a weak donor group and different furan derivatives responsible for withdrawing electrons (presenting a typical D-π−A molecular design). The compounds obtained for the need of this paper were originally synthesized, and their spectroscopic properties were described by Rémond et al.[48] These compounds have been selected due to their emission spectral range appearing in the first biological window and their ICT nature, boosting their potential applications in optoelectronics and laser light generation. Each of these compounds shows optical features, such as emission, in the biological range or a high value of molar absorption coefficient, which is beneficial to achieving inversion on population and consequently to obtain lasing. The properties presented in the mentioned publication[48] are desired in OLED applications and RLng-based light sources, while near-infrared (NIR) emission could be a key feature for further utilization in the developing biomedical industry. In addition, the synthesized dyes exhibit solid-state emission, suggesting that these molecules present active AIE properties.

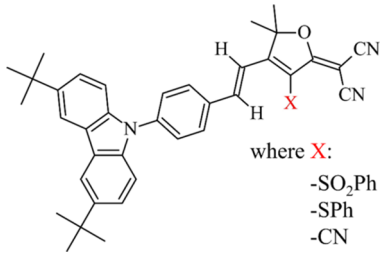

Figure 1. General formula of the studied dyes with hydrogen atoms is shown around the double carbon−carbon bond.

EXPERIMENTAL SECTION

Sample Preparation. Liquid samples were prepared by dissolving selected compounds in a tetrahydrofuran (THF) solution, with the final concentration reaching approximately $C \sim 1.5 \cdot 10^{-5}$ for the basic spectroscopic properties and $C \sim 1.5 \cdot 10^{-4}$ for the AIE measurements. The synthesis of the studied compounds was reported under the procedure described in ref 48.

Thin polymeric films with poly(methyl methacrylate) (PMMA) were fabricated by dissolving 100 μL of dye of 1.15 mg/mL dye/THF solution into a 300 μL 2% PMMA/THF mixture to achieve a final concentration concerning the polymer mass of ∼2% compound/PMMA (absolute concentration for all samples were 1.92%). The PMMA was obtained from Sigma-Aldrich, and its molecular weight is 120 kDa. It was used as received. To obtain polymeric samples, we utilized the drop-casting technique and subsequently dried them in a THF-rich atmosphere to slow the evaporation process and

https://doi.org/10.1021/acsomega.4c05484
ACS Omega 2024, 9, 40769−40782

enhance the quality of the resulting layers. The thickness values of the samples are 1.2 μm for SO2Ph, 3.7 μm for SPh, and 0.9 μm for −TCF.

These measurements were obtained using a deKTaK3 profilometer by averaging five measurements for each sample.

Optical Characterization. The absorption and emission measurements were recorded using a Jasco V-670 UV−vis−NIR spectrometer and Horiba FluoroMax 4 fluorescence spectrophotometer, respectively. The AIE studies were performed using the same setup.

Computational Details. All the DFT and time-dependent density functional theory (TD-DFT) calculations were performed with the latest version of Gaussian16 software.[49] The standard optimization procedure was improved, i.e., the default self-consistent field convergence criterion was increased to 10^{-10} a.u., and the optimization threshold was enhanced to 10^{-5} a.u. on average residual forces. In all DFT and TD-DFT calculations, the so-called ultrafine pruned integration grid (99 radial shells and 590 angular points per shell) was adopted. The ground-state and excited-state geometries (optimized structure and related vibrational analysis) were established using the Pople 6-31G(d) basis set, while vertical transitions were characterized by adapting more extensive basis -6-311+G(2d,p). In the first step, ground-state geometric parameters were optimized and followed by vibrational analysis, which confirmed that found structures, in fact, correspond to true minima on ground-state potential energy surfaces (PES); later, analogous characterization was performed for excited-state structures. Following the results of a recent excited-state properties benchmark treating a large number of real-life dyes, MN15[50] functional was chosen since it provides superior accuracy with respect to other well-known methods dedicated to charge transfer (CT) dyes (i.e., M06-2X, CAM-B3LYP or ωB97X-D).[51]

In order to account for the conditions of experimental measurements (here tetrahydrofuran solvent), all described calculations were performed using the polarizable continuum model (PCM)[52,53] in its linear-response (LR)[54,55] (optimization and vibrational analysis) or corrected-linear-response (cLR)[56] (vertical electronic energies) variants.

Finally, electron density difference (EDD) plots, together with charge transfer parameters, were estimated to gain additional insight into the character of the analyzed transitions. The above results were obtained using PCM-TD-MN15/6-311+G(2d,p), a theory-level adopting procedure proposed by Le Bahers and co-workers.[57] EDD plots were prepared using 0.002 a.u. In these graphs, the blue (red) areas indicate a density depletion (gain) upon photon absorption.

Thermal Investigation. Differential scanning calorimetry (DSC) was performed using a Du Pont 1090B apparatus with a heating/cooling rate of 20 °C·min^{-1} under nitrogen and using aluminum sample pans in the range of 0−320 °C. The glass transition temperature (T_g) was recorded in the second scan after cooling.

Electrochemical Investigations. Electrochemical properties were investigated by cyclic voltammetry (CV) and differential pulse voltammetry (DPV). The results were registered on Eco Chemie AutolabPGSTAT128n potentiostat using the platinum electrode as the working electrode with 0.1 mol/dm^3 Bu4NPF6 (Sigma-Aldrich) electrolyte and dichloromethane solution (Sigma-Aldrich) with 10^{-3} mol/dm^3 concentration. The platinum coil and silver wire were used as the auxiliary and reference electrodes, respectively. The moderate scan rate for cyclic voltammetry and differential pulse voltammetry was equal to 100 mV/s. The solutions were purged with argon before every measurement and performed at 24 ± 1 °C. The ferrocene couple (Fc/Fc^+) was used as the internal standard, and the EHOMO of Fc/Fc^+ was calculated to be equal to −5.1 eV, as shown in the publication.[58]

Organic Light-Emitting Diode. Devices with sandwich configurations ITO/PEDOT:PSS/compound/Al and ITO/PEDOT:PSS/compound:PVK:PBD/Al with 1, 2, and 15 wt % compound content in the blend were prepared. Devices were prepared on OSSILA substrates with pixilated ITO anodes and cleaned with detergent, deionized water, 10% NaOH solution, water, and isopropyl alcohol in an ultrasonic bath. Substrates were covered with PEDOT:PSS film by spin coating at 5000 rpm for 60 s and annealed for 5 min at 120 °C. The active layer was spin-coated on top of the PEDOT:PSS layer from a chloroform solution (10 mg/mL) at 1000 rpm for 60 s and annealed for 5 min at 100 °C. Finally, Al was vacuum-deposited at a pressure of $5 \cdot 10^{-5}$ Torr. Electroluminescence (EL) spectra were measured with the voltage applied by using a precise voltage supply (GwInstek PSP-405), and the sample was fixed to an XYZ stage. Light from the OLED device was collected through a 30 mm lens, focused on the entrance slit (50 μm) of a monochromator (Shamrock SR-303i), and detected using a CCD detector (AndoriDus 12305). Typical acquisition times were equal to 10 s. The prealignment of the setup was done using a 405 nm laser.

Random Lasing Measurements. For laser studies, we utilized the Surleite II Continuum third harmonic (λ = 355 nm) of a Nd:YAG nanosecond pulses laser (pulse duration τ = 5 ns, repetition rate f = 10 Hz) connected with the Optical Parametric Oscillator (Horizon, midband OPO by Continuum). The OPO was used to select the excitation wavelength corresponding to the maximum absorption for compounds tBuCBzSO2Ph, tBuCBzSPh, and tBuCBzTCF. The laser beam from the OPO was directed through to the half-wave plate and polarizer, which are used to keep the vertical and linear polarization of the beam and additionally to provide control over its intensity by rotation of the half-wave plate azimuth. Next, the excitation beam was carried out by a beam expanding system composed of two focusing lenses to form an "excitation stripe" and afterward fell on a regulated slit, responsible for the length of an excitation area. The samples were positioned behind the cylindrical lens focal point, which was placed close to the regulated slit. The laser emission from the probes was collected by a fiber connected to an Andor Shamrock SR-500i spectrometer equipped with an AndoriDus CCD camera. All of the measurements concerning lasing threshold determination were carried out for "excitation stripes" of 0.83 cm in length and 0.03 cm in height for all of the studied compounds.

RESULTS

This section is divided into parts. The first one describes the results of basic spectroscopic, thermal, and electrochemical analysis. The second section refers to potential applications for the development of OLEDs and laser device development.

Basic Spectroscopic Properties and Thermal and Electrochemical Analysis. *Quantum-Chemical Calculations.* First, we aimed to explore quantum-chemical calculations to gain insight into the photophysics of the studied molecules and to verify the occurrence of ICT. The calculations were performed using the time-dependent density functional theory (TD-DFT) approach. All details about the

https://doi.org/10.1021/acsomega.4c05484
ACS Omega 2024, 9, 40769−40782

Table 1. Experimental and Calculated Spectroscopic Parameters[a,b]

	theory							experiment				
compound	λ_{abs} (nm) $S_0 \rightarrow S_1$	f $S_0 \rightarrow S_1$	λ_{abs} (nm) $S_0 \rightarrow S_3$	f $S_0 \rightarrow S_3$	λ_{emi} (nm) $S_1 \rightarrow S_0$	f $S_1 \rightarrow S_0$	$\Delta\lambda$ (nm)	λ_{abs} (nm)	ε (M^{-1} cm^{-1})	λ_{emi} (nm)	$\Delta\lambda$ (nm)	fwhm (nm)
tBuCBzSO$_2$Ph	**512**	**1.19**	**366**	**0.67**	**603**	**1.60**	**92**	489	51,500	653	164	126
tBuCBzSPh	**467**	**1.14**	**349**	**<0.05**	**612**	**1.52**	**145**	453	39,230	618	165	114
	460	1.11	349	0.39	554	1.53	94					
tBuCBzTCF	**523**	**1.15**	**377**	**0.50**	**595**	**1.62**	**72**	487	50,550	649	162	136
	523	1.15	377	0.50	598	1.54	75					

[a]In the theoretical part, the λ^{abs} and λ^{emi} are vertical energies computed at the MN15-cLR-PCM theory level. $\Delta\lambda$ denotes the Stokes shifts. [b]The values corresponding to more stable conformers are marked with bold font.

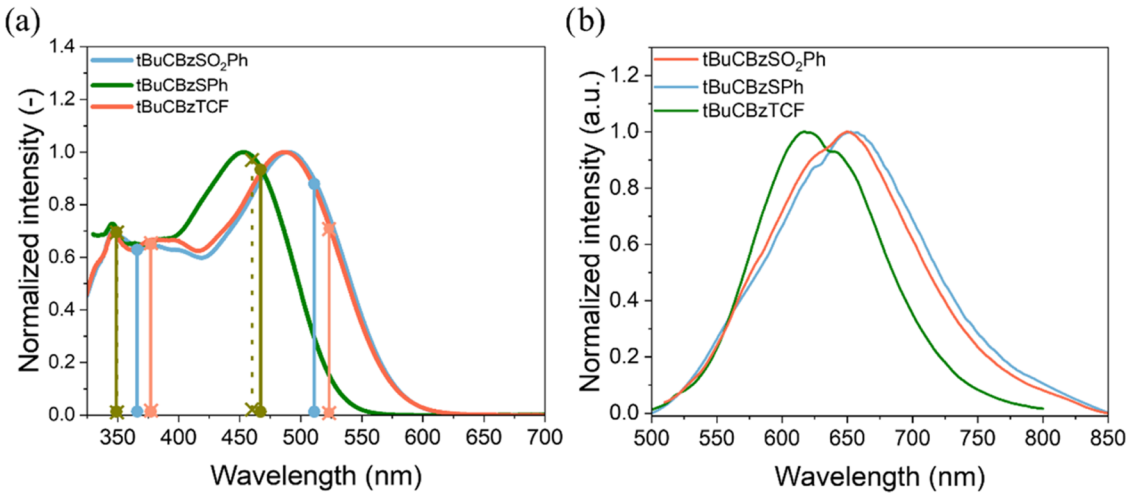

Figure 2. Experimental absorption (a) and emission (b) spectra of investigated compounds in THF solution $C \sim 1.5 \times 10^{-5}$ mol/dm^3. The emission spectra were recorded at room temperature using an excitation wavelength equal to the maximum absorption for each compound. Vertical lines indicate maxima computed for S0 → S1 and S0 → S3 transitions calculated by the TD-DFT approach (the details can be found in the Experimental Section). The continuous lines with dots at the ends represent more stable conformers, while dashed lines with crosses at the ends are less stable conformers. Inset in part a shows the molecular structure of investigated compounds.

computational protocol employed here are described in the Experimental Section.

Characterization of the investigated compounds started by checking whether they had more than one stable rotamer in the tetrahydrofuran (THF) solution by rotating the acceptor moiety (SO_2Ph, SPh, and TCF) two stable structures for each compound were identified. In more detail, the most stable conformers have the functional groups ($-SO_2Ph$, $-SPh$, and $-CN$, respectively) pointing "up" (for details, see the electron density difference (EED) plots in Table 2). The difference in Free Gibbs energy (ΔG) between respective rotamers ranges from 0.01 for the TCF dye up to 2.7 kcal/mol reported for the SO_2Ph derivative (See Table S1 in SI). On the ground of Boltzmann distribution and assuming room temperature, both rotamers of tBuCBzTCF and tBuCBzSPh dyes can be present in the solution. In contrast, the probability of observing another conformer of tBuCBzSO$_2$Ph is negligible ($\ll$1%). Consequently, two rotamers were included in the further analysis for tBuCBzTCF and tBuCBzSPh only.

The selected computational protocol correctly describes the photophysics of the studied compounds. TD-DFT results were compared with measured spectroscopic parameters (Table 1 and Figure 2). As depicted in Table 1, the MN15 functional can satisfactorily reproduce spectral features of absorption bands, including general shape as well as maxima position. Notably, the predicted position of absorption maxima is slightly overestimated (in the case of tBuCBzTCF to the larger extent, ca. 30 nm), yet the absolute errors (AE) are in the acceptable range of 0.04−0.11 eV. In turn, larger deviations from experimental values were observed for emission spectra, i.e., tBuCBzTCF and tBuCBzSO$_2$Ph bands are ca. 50 nm (AE < 0.2 eV) underestimated while predicted tBuCBzSPh band position differs only negligibly (6 nm). Such discrepancies fully coincide with the strong charge transfer (CT) character of examined transitions. This overestimation in absorption and emission spectra may be caused by several reasons; for instance, the computational model assumes ideal conditions, whereas the complexity of the real systems might be higher. For example, the interactions with solvent were modeled using the PCM method, which is accurate only for averaged electrostatic interactions. Besides, compounds with charge transfer characteristics are also very sensitive to environmental changes like temperature or the solvent's hygroscopic properties, etc., which may impact the measured absorption spectra. It is worth highlighting that we can observe the difference between two stable conformers in the THF for the SPh dye. Therefore, even the conformational differences might contribute to discrepancies in both values. Although some differences between the predicted and actual values are observed, the overall fit of the results is satisfactory.

The TD-DFT analysis confirmed that the main absorption bands correspond to the $S_0 \rightarrow S_1$ transitions, while weaker

https://doi.org/10.1021/acsomega.4c05484
ACS Omega 2024, 9, 40769−40782

Table 2. Electron Density Difference (EDD) Plots and Related $S_0 \rightarrow S_1$ Electron Transition Parameters of Examined Compounds − d_{CT} Stands for Charge Transfer Distance, q_{CT} is the Total Transferred Charge, μ_{ES}-μ_{GS} Represents the Difference in Dipole Moment Magnitude between the Ground and Franck−Condon Region of the Excited State[a]

Cmpd	EDD	μ_{ES}-μ_{GS}[D]	d_{CT}[Å]	q_{CT}[e]
tBuCBzSO$_2$Ph	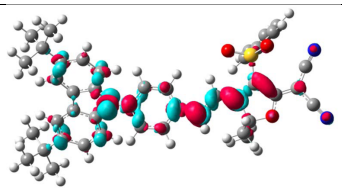	23.59	5.31	0.96
tBuCBzSPh	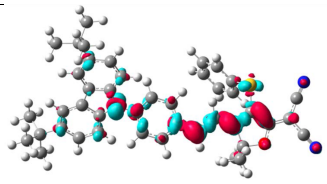	17.31	4.67	0.80
	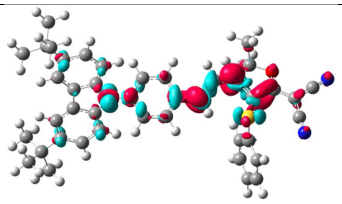	16.70	4.42	0.81
tBuCBzTCF	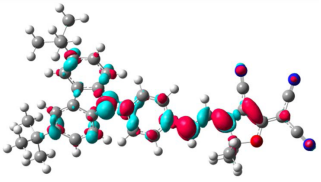	22.62	5.40	0.93
	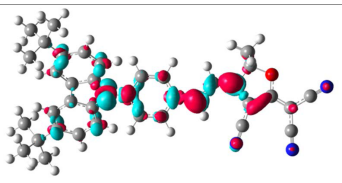	21.33	5.25	0.90

[a]In the EDD, the blue (red) color marks electron density depletion (gain) upon photon absorption. The contour value was set to 0.002 a.u.

bands around 350 nm coincide with $S_0 \rightarrow S_3$. Lowest-lying $\pi-\pi^*$ excitations of all of the examined structures are characterized by large oscillator strengths (varying from 1.11 to 1.19), while oscillator strengths corresponding to $S_0 \rightarrow S_3$ transitions are significantly lower (0.39−0.67). For all dyes, the largest contributions in the main transitions can be ascribed to one-electron HOMO−LUMO excitation; however, non-negligible fractions from the HOMO−2 to LUMO transition are also present. As expected, the computational protocol attributed the emission bands to $S_1 \rightarrow S_0$, but the ascribed oscillator strengths are much higher (1.52−1.62).

To gain insight into the nature of the lowest-lying $\pi \rightarrow \pi^*$ transitions, we assessed related CT parameters. As can be seen from EED plots (see Table 2), the carbazole unit acts as an electron donor, while furan-based moieties serve as an electron acceptor for all examined derivatives, which is consistent with our preliminary assumptions concerning D-π−A design. Notably, no change in electron density is observed within tBu groups or phenyl rings attached to sulfur atoms. It should be highlighted that all examined transitions displayed a strong CT nature, which is reflected by the substantial change in the dipole moment (μ_{ES}-μ_{GS}), reaching above 20 D for tBuCBzSO$_2$Ph and tBuCBzTCF as well as high total transferred charge (q_{CT}) values. As can be seen, the donor and acceptor moieties of examined dyes are connected with an extended π-conjugated spacer; thus, all molecules are also characterized by high charge transfer distance (d_{CT}) (>4 Å). Notably, among the series tBuCBzSPh presents significantly lower (yet still meaningful) CT parameters (μ_{ES}-μ_{GS}, q_{CT}, and d_{CT}) than the other two dyes.

AIE. To test whether the investigated compounds exhibit AIE, different fractions of THF solution ($C \sim 1.5 \times 10^{-4}$ mol/dm^3) were mixed with water. By increasing the water/THF ratio, aggregation of the investigated dyes was forced, as

https://doi.org/10.1021/acsomega.4c05484
ACS Omega 2024, 9, 40769−40782

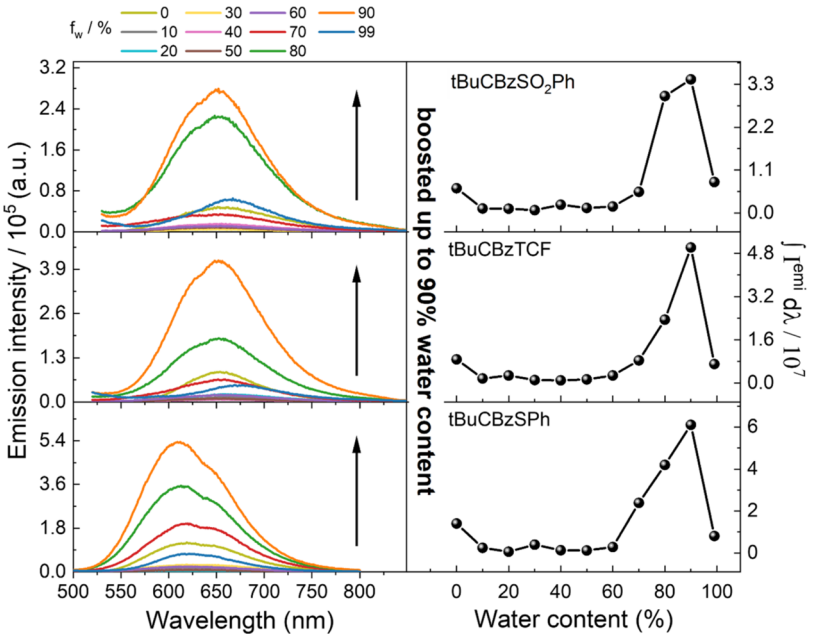

Figure 3. Impact of water addition on the emission intensity (left panel) and dependence on water. Water fraction (f_w/%) on integrated emission spectra ($\int I^{emi} d\lambda$) taken from the above (right panel) for the studied compounds.

Table 3. Electrochemical Data with the E_{red}, E_{ox}, and Onset Potentials (vs. Fc/Fc$^+$) and an Energy Band Gap E_g[a]

molecule	method	E_{red} [V]	$E_{red}^{(onset)}$ [V]	E_{ox} [V]	$E_{ox}^{(onset)}$ [V]	EA [eV]	IP [eV]	E_g [eV]
tBuCBzSO$_2$Ph	CV	−1.13[b]	−1.01	0.80[c]	0.67	−4.09	−5.77	1.68
	DPV	−1.11	−1.00	0.74	0.65	−4.10	−5.75	1.65
tBuCBzSPh	CV	−1.46[b]	−1.38	0.76[c]	0.64	−3.72	−5.74	2.02
	DPV	−1.39	−1.31	0.69	0.61	−3.79	−5.71	1.92
tBuCBzTCF	CV	−1.16[b]	−1.05	0.78[c]	0.62	−4.05	−5.72	1.67
	DPV	−1.22	−1.13	0.73	0.57	−3.97	−5.67	1.70

[a]IP = $(-5.1\text{-}E_{ox}^{(onset)}) \cdot e^-$, EA = $(-5.1\text{-}E_{red}^{(onset)}) \cdot e^-$, $E_g = E_{ox}^{(onset)}\text{-}E_{red}^{(onset)}$. Solvent: CH_2Cl_2 with $c = 10^{-3}$ mol/dm^3 and electrolyte 0.1 mol/dm^3 Bu_4NPF_6 and platinum wire (Pt) as a working electrode. [b]Irreversible process. [c]*Quasi*-reversible process. E_{ox}− the first oxidation process, E_{red}− the first reduction process, $E_{red}^{(onset)}$ − the onset potential of the first reduction process, $E_{ox}^{(onset)}$− the onset potential of the first oxidation process. IP and EA as ionization potential and electron affinity. The Fc/Fc$^+$ was used as the internal standard.

investigated dyes are not soluble in water.[59] Figure 3 presents the emission intensity and the evolution of photoluminescence spectra with respect to the water fractions (f_w/%) for each compound. It is clearly visible that all compounds are AIE-active. The emission was recorded for excitation at the maximum of the absorption wavelength (see Table 1); the spectral emission was collected in the 550−850 nm range for the tBuCBzSO$_2$Ph and tBuCBzSPh while for compound tBuCBzTCF from 550 to 800 nm. At the origin of the nonsolvent addition, we observed a slightly lower integrated intensity of the emission spectra (see Figure 3). It can be explained by the higher polarity of mixed solvents and dilution of the resulting dye/solvent/nonsolvent mixture.[60] A significant enhancement in the emission intensity emerged at water content approaching 60−70%, depending on the investigated dye, appointing the threshold value for which aggregation occurs. Maximum emission intensities are reached when the water fraction is 90% for all three dyes, with enhancement factors equal to 5.4, 4.3, and 5.7 (relative to pure THF solution) for tBuCBzSO$_2$Ph, tBuCBzSPh, and tBuCBzTCF, respectively. The emissions intensity decreases drastically for the 99% water/THF mixture due to a substantial quantity of nonsolvent and sedimentation processes.

Interestingly, for tBuCBzSO$_2$Ph and tBuCBzTCF, we can see that emission in the AIE experiment is positioned around ∼650 nm. For the highest water addition (∼99%), we see a slight red emission shift in both cases with respect to no water content (Figure S1 in the SI). In the case of the tBuCBzSPh dye, the AIE behavior is also present; however, the explanation of the emission nature is not clear-cut. It is undoubtedly evident that in the last case aggregates play an important role in emissions intensity; nevertheless, the shape of the spectrum remains almost unchanged (see Figure S1 in SI).

Thermal Investigations. The thermal characteristics were determined using differential scanning calorimetry (DSC) as described in the Experimental Section. In the first heating scan, the endothermal peaks of the melting temperature (T_m) in the 306−327 °C range were registered. The compound tBuCBSO$_2$Ph was characterized by the highest T_m. In the second heating scan, the glass transition temperature (T_g) at 158 °C (tBuCBSO$_2$Ph), 138 °C (tBuCBzSPh), and 223 °C (tBuCBzTCF) was detected. In the case of tBuCBzTCF, after T_g, during further heating, the cold crystallization temperature (T_{cc} = 240 °C) and the melting temperature (T_m = 312 °C) were observed. For compounds tBuCBSO$_2$Ph and tBuCBzSPh, the lack of T_{cc} and T_m was noticed. The presence of the glass transition temperature is characteristic of molecular glasses,

https://doi.org/10.1021/acsomega.4c05484
ACS Omega 2024, 9, 40769−40782

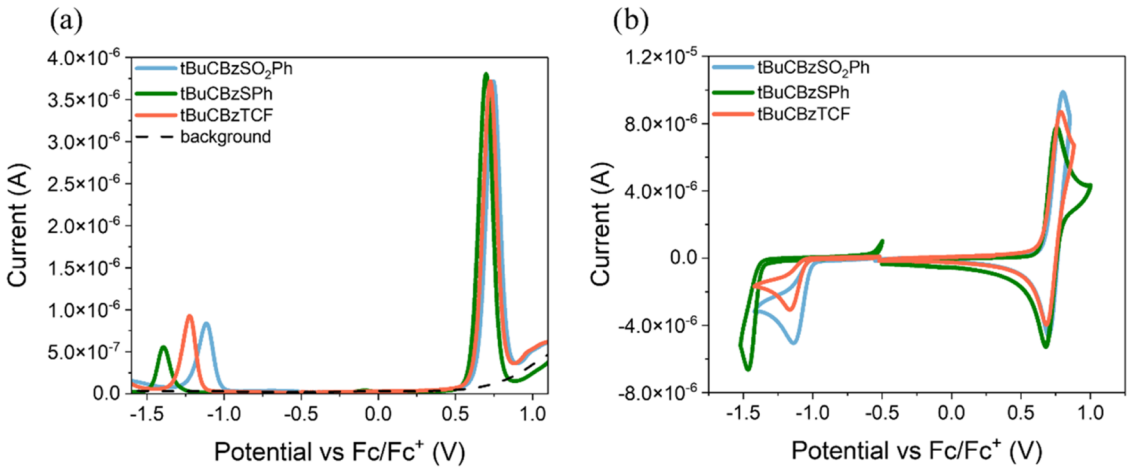

Figure 4. Voltammograms measured with DPV (a) and CV methods (b).

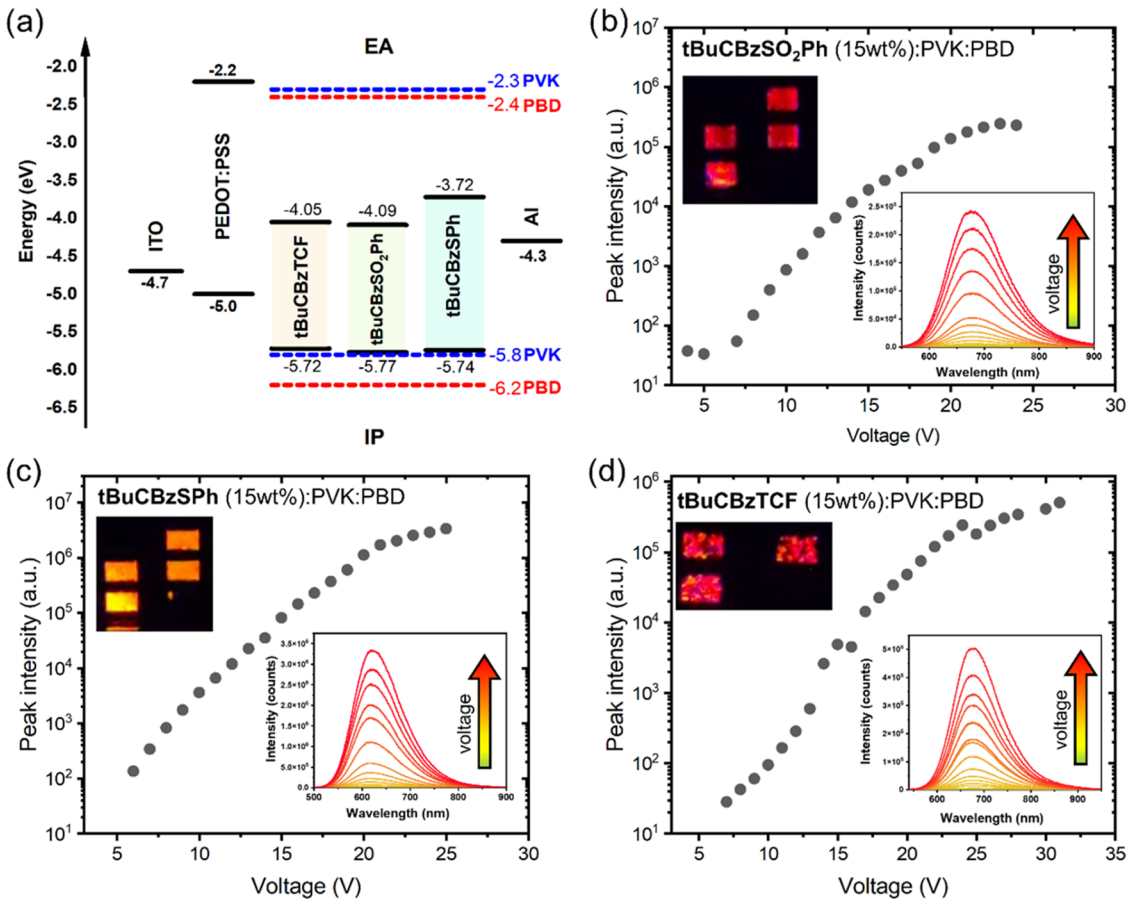

Figure 5. Energy diagram for all of the materials used in OLED devices and their typical design (a). Electroluminescence peak intensities of OLEDs vs applied voltage for $tBuCBzSO_2Ph$ (b), tBuCBzSPh (c), and tBuCBzTCF (d) doped on the PVK: PDB matrix at 15 wt %. Insets are showing the evolution of electroluminescence spectra upon increasing voltage and real photographs of OLED emission.

where the amorphous glass is formed via a supercooled liquid of the crystalline compound (T_m in the first heating scan). Results from DSC measurements are shown in Figure S2 in the SI. To summarize, all compounds showed high melting and glass transition temperatures required for optoelectronic applications.

Electrochemical Properties. The electrochemical investigations were performed (as described in the Experimental Section) in a dichloromethane solution with a concentration equal to 10^{-3} and 10^{-1} mol/dm^3 Bu_4NPF_6 electrolyte. The electrochemical data from the cyclic voltammetry (CV) and differential pulse voltammetry (DPV) measurements are collected in Table 3, and the voltammograms are presented in Figures 4 and S3. The onset potentials from the first oxidation and reduction processes were used to calculate the ionization potentials (IP) and electron affinities (EA).

The investigated compounds in the solution were electrochemically active, and the reduction and oxidation processes

https://doi.org/10.1021/acsomega.4c05484
ACS Omega 2024, 9, 40769−40782

Table 4. Electroluminescence Data[b]

the active layer structure	device parameters		
	λ_{EL}[a](nm)	EL_{Max}[a](counts)	$U_{EL,Max}$[c](V)
tBuCBzSO$_2$Ph	716	354,827	26
tBuCBzSO$_2$Ph(1 wt %):PVK:PBD	629	233,057	25
tBuCBzSO$_2$Ph(2 wt %):PVK:PBD	608	9836	12
tBuCBzSO$_2$Ph(15 wt %):PVK:PBD	675	242,598	23
tBuCBzSPh	655	4,805,200	20
tBuCBzSPh(1 wt %):PVK:PBD	600	597,191	26
tBuCBzSPh(2 wt %):PVK:PBD	600	8519	22
tBuCBzSPh(15 wt %):PVK:PBD	619	3,341,700	25
tBuCBzTCF	711	2192	15
tBuCBzTCF(1 wt %):PVK:PBD	638	233,743	31
tBuCBzTCF(2 wt %):PVK:PBD	654	5266	22
tBuCBzTCF(15 wt %):PVK:PBD	676	504,400	33

[a]λ_{EL} − maximum of the electroluminescence band. [b]EL_{Max} − maximum intensity at λ_{EL}. [c]$U_{EL,Max}$ − external voltage for the maximum electroluminescence intensity. The PVK:PBD ratio 50:50 wt %.

were registered. The first irreversible reduction process was noticed in the range of −1.46 to −1.11 V vs Fc/Fc$^+$ (cf. Table 2), and the first quasi-reversible oxidation process was detected in the range of 0.80−0.69 V vs Fc/Fc$^+$ for the studied dyes. The presence of the acceptor groups, such as −CH═C(CN)$_2$ moieties, allowed the registration of the reduction process (cf. Figure 4). The reduction process was the easiest for tBuCBzSO$_2$Ph and the most difficult for tBuCBzSPh. In the case of tBuCBzTCF, two reduction peaks were recorded, one at E_{red} = −1.22 V vs Fc/Fc$^+$ and the other at E_{red} = −1.66 V vs Fc/Fc$^+$(cf. Figure S3), which is associated with the presence of the third group −CN. The oxidation process is related to the presence of the donor elements of the molecule, such as carbazole.[61] Similar oxidation potentials (as well as $E_{ox}^{(onset)} \approx$ 0.63 V vs Fc/Fc$^+$) were recorded for the tested compounds at about E_{ox} = 0.75 V vs Fc/Fc$^+$ and the second irreversible oxidation peak also shows a similar value (E_{ox} about 1.40 V vs Fc/Fc$^+$), indicating oxidation of the carbazole group (cf. Table 3[62]). The carbazole is known as a structure that can undergo polymerization.[19] However, the carbazole is substituted at the 3N position, which may inhibit the polymerization process. This possibility was also checked, although no polymer formation was observed. The electrochemical investigations were also repeated using a GC (glassy carbon) working electrode in the DPV method. The differences between the potentials measured with the Pt electrode and the GC electrode were within the 0.1 V range. Based on the onset potentials, as mentioned above, the IP and EA energy levels were calculated. The IP values were similar for the investigated compounds (in the range of −5.75 to −5.67 eV), as well as the EA values in the case of tBuCBzSO$_2$Ph and tBuCBzTCF (−4.10 to −3.97 eV). However, the EA values of tBuCBzSPh were higher (−3.79 to −3.72 eV). The presented compounds are characterized by a low energy band gap (2.02−1.65 eV), which is desirable in optoelectronic applications.

Potential Applications. *OLED Devices.* The investigated compounds were used as the active layer in the device structures ITO/PEDOT:PSS/compound/Al and ITO/PEDOT:PSS/compound:PVK:PBD/Al, the fabrication details of which can be found in the Experimental Section. The guest−host active layer structure was constructed with the three components: compound:PVK:PBD (PVK:PBD binary matrix ratio 50:50 wt %). The poly(9-vinylcarbazole) (PVK) and 2-(4-*tert*-butylphenyl)-5-(4-biphenylyl)-1,3,4-oxadiazole (PBD) were used respectively as a hole and an electron conductive material. The measurements were conducted for compound content in the active layer equal to 1, 2, and 15 wt %, as well as for neat-dye films sandwiched between the PEDOT:PSS layer coated on the ITO and Al layer. A schematic representation of the design of an OLED with ionization potentials and electron affinities of used materials is shown in Figure 5a. The presented diodes emit light from yellow (λ_{EL} = 600 nm), orange (λ_{EL} = 608−629 nm), and red (λ_{EL} = 638−716 nm) spectral regions under minimum external voltage between 6 and 10 V, depending on the OLED composition. The reason that underlies the utilization of high driving voltage for the studied compounds can be caused by the thickness of the layers and lack of the exciplex formation, which ensures a general carrier injection barrier or limitation resulting from molecular design.[63−65] Based on the emission intensity vs applied voltage plots, we were able to identify the applicability of investigated compounds in the fabrication of OLEDs. Comparing Figures S6c and 5, we see a similar OLED performance for tBuCBzSPh doped to PVK:PBD in the amount of 15 wt % and a neat film. The highest electroluminescence intensity was observed for a device with a neat tBuCBzSPh and under an external voltage of 20 V (cf. Table 4); however, the device degrades at lower voltages. On the other hand, for moderate voltages (9−16 V), the emission intensity is higher for 15 wt % of dye in the PVK:PBD layer. In almost all cases, the tBuCBzSPh compound has shown superiority over other dyes in the performance of the OLED, as presented in Figures 5c and S6−S8.

The exception from this observation can be noticed for the 2 wt % of dye loadings to PVK:PDB matrices, where the highest intensity was observed for tBuCBzSO$_2$Ph dye. However, in this case, the device based on the tBuCBzSO$_2$Ph compound degraded rapidly after crossing only the 12 V of applied voltage (cf. Figure S9 and Table 4). For 1 wt % of dye concentration, the devices with tBuCBzSO$_2$Ph and tBuCBzSPh performed similarly, but finally, the second one was able to reach higher output intensity at higher voltage values, which is depicted in Figure S9 and in Table 4. In the case of tBuCBzSO$_2$Ph and tBuCBzSPh compounds, a high loading at 15 wt % results in nearly identical performance of the devices fabricated using only a neat film of dyes. However, for tBuCBzTCF, the PVK:PBD matrix improves the performance of the OLED (cf. Table 4 and Figure S6d). Typically, what can be seen from

https://doi.org/10.1021/acsomega.4c05484
ACS Omega 2024, 9, 40769−40782

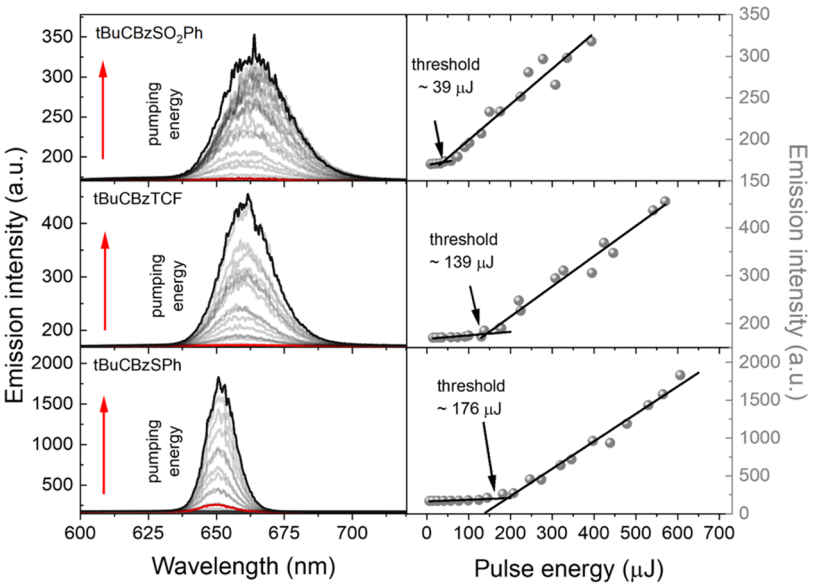

Figure 6. Evolution of the emission spectra with increasing pumping energy for PMMA layers doped with ∼2% of the studied compounds. Narrow modes typical for coherent RLng are visible for all samples (left panel), presented as a gray and transparent continuous line and black line at the top of the spectra related to the maximum of the utilized laser pump energy. Red lines represent the value of the laser threshold. Charts on the right show the corresponding peak intensity dependence on pumping energy with typical RLng inflection points indicating the lasing threshold.

Table 4, Figures 5, S7 and S9 is the red shift of emission spectra with increasing loadings, with the greatest one reported for neat films. A combination of this behavior and OLED performances indicates the positive influence of the AIE effect on electroluminescence.

The maximum wavelength of pristine PVK:PBD absorption (shown in Figure S4) is located at 410 nm. The large shifts in absorption and emission wavelengths for dye-doped matrices presented in Figures S4 and S5 and described in Table S2 suggest the energy transfer from the matrix to the host. The location of the estimated IP energy level of the compounds oscillates around the IP level of the matrix (cf. Figure 5a). Due to the location of the IP and EA of the compounds used in the presented devices, the energy transfer and the trapping mechanism may coexist.

Furthermore, we also observed that the performance of devices can be changed by the amount of dye dopant and the wavelength of emission. For example, in the case of tBuCBzSO$_2$Ph and tBuCBzTCF, we are able to shift the emission into the biological window by increasing the dye concentration. For neat films, the emission from tBuCBzSPh is also in the biological window region. Notably, the emission can even reach the NIR range for other compounds.

Lasing. The laser emission was investigated using a nanosecond laser-based optical system as described in the Experimental Section. For those measurements, we utilized polymeric asymmetric slab waveguides/quasiwaveguides made of poly(methyl methacrylate) (PMMA) deposited on microscopic support glass slides. Samples contained a constant concentration of each compound (∼2% dye with the polymer). All samples were prepared via the drop-casting method (see the Sample Preparation section). PMMA was chosen due to its well-known properties and good optical quality.[30] The pumping wavelength was set to the maximum of the absorption spectra measured for the thin films for all examined compounds (λ^{abs}tBuCBzSO$_2$Ph = 503 nm, λ^{abs}tBuCBzSPh = 455 nm, λ^{abs}tBuCBzTCF = 490 nm—note that all of them are slightly red-shifted with respect to liquid solutions see Figure S10). As displayed in Figure 6, the emission spectra of all dyes are characterized by narrow and high spikes appearing in a random fashion after the pumping energy reaches the threshold of laser action. The visualization of this parameter was presented as a red line inside each emission spectra. The threshold value was calculated using a well-known method, namely the light−in−light−out (Li-Lo).[66] The rapid growth of the emission intensity corresponds to the development of laser emission from the photoluminescence spectra, resulting in a significant increase in the emission intensity. These changes can be represented as points, and the two straight lines drawn through them, which intersect at the inflection point, represent the value of the random laser threshold. The described phenomenon is correlated with coherent random lasing.[67] The formation of the spikes is associated with the interference effect of the light trapped inside the closed loop in the scattering media occurring in the sample. This effect enhances the amplification of specific modes, resulting in a narrow spike observation. The RLng was observed for all studied compounds at bands located at around ∼665 nm for tBuCBzSO$_2$Ph and tBuCBzTCF and 655 nm for tBuCBzSPh. The full width at half-maximum (fwhm) of whole photoluminescence bands collapsed from approximately 126, 136, and 114 nm when threshold conditions were reached around 28.5, 22.0, and 12.6 nm, respectively. Typically, in organic dyes, a huge number of oscillatory states ensure the 4-level system of laser operation. The internal conversion speed within the ground electronic state determines between which states the population inversion can appear and thus determines the shape of the gain profile. Indeed, the polymeric layer with tBuCBzSPh shows the smallest fwhm of RLng; however, at this stage of research, it is impossible to determine whether this observation is due to the slowest internal conversion within the ground electronic state or to the limited waveguiding. The threshold conditions of laser emission in the case of the tBuCBzSO$_2$Ph dopant were found to be around 39 μJ/pulse, which is the lowest reported in this study. The tBuCBzTCF doped system is characterized by an energy threshold of

https://doi.org/10.1021/acsomega.4c05484
ACS Omega 2024, 9, 40769−40782

around 139 μJ/pulse, while for tBuCBzSPh, this value is equal to 176 μJ/pulse. Assuming the Gaussian shape of pulses, the mentioned values correspond to the following peak powers: 7.3, 26.1, and 33.1 kW.[68]

DISCUSSION

Theoretical calculations largely contribute to rationalizing the CT nature of the studied molecules: the changes in the calculated dipole moment vary between 16.70 and 23.59 D, depending on the molecule and its geometry. Interestingly, tBuCBzSPh exhibits significantly lower CT parameters, i.e., μ_{ES}-μ_{GS} decreased to ∼17D with respect to the two other derivatives (cf. Table 2), which can be attributed to the large electron density depletion "orb" localized on the sulfur atom of the EDD plot. Therefore, the SPh moiety can be viewed as a weak secondary donor unit attached directly to the electron-accepting dihydrofuran unit, thus impeding the charge transfer along the molecular axis. As a result, it shows the smallest red shift of emission and molar extinction coefficient (cf. Table 1). For $-SO_2Ph$ and −TCF moieties, the CT character is rather similar, which is reflected in nearly identical calculated μ_{ES}-μ_{GS} values as well as comparable positions of the absorption and emission spectra.

The very strong CT character of the investigated molecules leads to a significant red-shifted emission. Particularly, for the $-SO_2Ph$ and −TCF compounds, emission reaches the short-wavelength edge of the biological window. Moreover, the formation of the aggregates can cause a further red-shift of the photoluminescence, as was reported for pure dye films (reaching the NIR region) and PVK:PBD matrices with the highest dye loadings (15%). Consequently, those two compounds are even better suited for biological applications.

Furthermore, all of the investigated dyes exhibit AIE behavior. In general, the issues associated with quenching during aggregation are common problems with the implementation of organic dyes, especially in the biological field. For instance, protein aggregation is correlated with numerous human diseases, such as cancers and neurodegenerative or metabolic disorders.[69] Using AIE-based organic dyes, such as those presented in this study, to monitor unwanted protein changes using various methods can overcome the mentioned limitations and lead to increased efficiency in detecting pathological changes within the organism. Nevertheless, the existence of aggregates can shift the emission toward biological windows and significantly increase the emission intensity, facilitating potential future applications in medical sciences.

As was mentioned before, all the compounds show relatively small band gap values, which is a frequently desired feature for the construction of OLEDs. Several types of OLED devices were prepared. In general, a higher value of the electroluminescence peak was obtained for the tBuCBzSPh compound. It is worth mentioning that recently, the intensity of the emission was proposed as a significant property for the use of OLEDs, especially when we consider the transmission of light through the skin. As was previously reported, for red OLEDs, the transmitted light was approximately 46% of the initial intensity of electroluminescence.[70] The mentioned parameter can be beneficial in various types of advanced and smart wearables containing OLEDs, such as in cutaneous wound healing[62] or smart textiles as a proposition for clothing capable of responding to emergencies or providing ubiquitous healthcare.[71] On the other hand, the weakest performance was reported for the TCF moiety, which is in accordance with emission quantum yield measurements described by Rémond et al. for solid-state emission.[48] This observation once again shows that the AIE effect can play a beneficial role in optoelectronic device construction, which is required for biological applications. The investigated dyes can perfectly match the wavelengths desired for the development of novel, organic-based pulse oximeters[10] or as a light source for stimulating gene expression for tumor suppression, which has a positive impact on the aging pathway.[72]

Finally, we observed RLng emission from dye-doped polymeric layers at wavelengths that can be linked to the emission of aggregates. The random nature of laser emission is possibly the result of the enchanted light scattering from aggregates as well as layers' irregularities (characteristic of the drop-casting technique). The energy thresholds were estimated to be moderate for organic dyes; however, there is still room for further optimization, for example, by applying different types of high-quality resonators or by optimizing the polymeric system (thickness, type of polymer, dye concentration, etc.). However, the threshold conditions shown here are still relatively low for obtaining lasing, for example, by using a cheap DPSS laser operating in the pulse regime as pumping sources. It is worth noting that the laser threshold value is a crucial parameter of any laser device's performance. For instance, besides the abovementioned application of the DPSS laser, a low laser threshold stands for the ability to operate with less input pump power; thus, it can be beneficial, for example, in the application where the value of the used power pump is crucial in advanced optoelectronic devices,[73] portable sensors,[74] microlasers,[75] or even as a part of the integrated OLED devices as a pumping electrically driven organic semiconductor laser.[76]

In general, the energy threshold level is an intricate function related to rate equations, dependent on emission quantum yield, emission lifetime, absorption coefficients, speed of different transitions, resonator quality factor, etc. Therefore, the observed threshold conditions cannot be simply explained in terms of the emission quantum yields. However, we can see some coincidences with the extinction coefficient. For example, the lowest threshold was reported for $tBuCBzSO_2Ph$, for which we observe the highest ε and moderate emission quantum yield. Next, a slightly higher threshold was reported for tBuCBzTCF. In this case, ε is slightly lower than that for $tBuCBzSO_2Ph$, but its quantum yield of emission is the lowest.[17] Finally, for tBuCBzSPh, the threshold conditions are the highest. This behavior can be explained in terms of the relationship between the absorption and gain coefficients. First, the dye with the lowest ε cannot absorb as much light as other dyes; thus, the pumping is less efficient. Second, as the gain coefficient can be seen as a negative absorption coefficient, the potential gain is determined by absorption. Therefore, the interplay between the ε value and emission quantum yields can qualitatively explain the observed coincidence.

Finally, it is worth highlighting that the emission range located between 600 and 700 nm is reported in the literature as an ideal wavelength, for instance, for photodynamic therapy (PDT) due to its deep tissue penetration while simultaneously avoiding overlap with the absorption peaks of water and oxygenated hemoglobin.[77] In this context, OLEDs having electroluminescence in the red region of the light are suitable for all purposes correlated with the PDT, where light and a specialized photosensitizer are used to create a reactive form of oxygen capable of killing bacteria in its surroundings.[78,79] On

https://doi.org/10.1021/acsomega.4c05484
ACS Omega 2024, 9, 40769−40782

the other hand, RLs are also well-known for their application in medicine, as was previously mentioned. For example, RLs can detect early-stage tumors or can be used in the field of automated laser surgery systems.[80]

CONCLUSIONS

In conclusion, the investigated dyes show a remarkable red shift in emission due to the ICT effect and formation of aggregates. The OLED emission and RLng can be obtained in the NIR region of light, indicating the usefulness of the investigated dyes for biological purposes. The presence of the AIE phenomenon allowed more flexible functionalization of guest−host systems using higher loads of dye-dopants as well as designing devices based only on neat-dye films, highly influencing the optical properties of the resulting system. Thus, by simple concentration changes, it is possible to tune the emission properties of the resulting OLED device. In both cases (OLEDs and RL), we obtained significant luminescence intensities for wavelengths characteristic of the biological window, which paves the way for the further utilization of dyes described here in biomedical research and applications. Finally, there is still room for optimizing RL samples and the design of an OLED to improve the performances of both types of devices.

ASSOCIATED CONTENT

Supporting Information

The Supporting Information is available free of charge at https://pubs.acs.org/doi/10.1021/acsomega.4c05484.

Additional data, and a table with more comprehensive information, facilitating a deeper understanding of the study's findings (PDF)

AUTHOR INFORMATION

Corresponding Authors

Kamila Lupinska − *Institute of Advanced Materials, Faculty of Chemistry, Wroclaw University of Science and Technology, 50-370 Wroclaw, Poland;* orcid.org/0000-0002-6441-2085; Email: kamila.lupinska@pwr.edu.pl

Lech Sznitko − *Institute of Advanced Materials, Faculty of Chemistry, Wroclaw University of Science and Technology, 50-370 Wroclaw, Poland;* orcid.org/0000-0002-7013-7999; Email: lech.sznitko@pwr.edu.pl

Authors

Sonia Kotowicz − *Institute of Chemistry, University of Silesia, 40-006 Katowice, Poland;* orcid.org/0000-0001-6021-0892

Anna Grabarz − *Institute of Advanced Materials, Faculty of Chemistry, Wroclaw University of Science and Technology, 50-370 Wroclaw, Poland; Department of Physical and Theoretical Chemistry, Faculty of Natural Sciences, Comenius University, 84215 Bratislava, Slovakia*

Mariola Siwy − *Centre of Polymer and Carbon Materials, Polish Academy of Sciences, 41-819 Zabrze, Poland*

Karolina Sulowska − *Institute of Advanced Materials, Faculty of Chemistry, Wroclaw University of Science and Technology, 50-370 Wroclaw, Poland; Institute of Physics, Faculty of Physics, Astronomy and Informatics, Nicolaus Copernicus University, 87-100 Torun, Poland;* orcid.org/0000-0002-7905-6642

Sebastian Mackowski − *Institute of Physics, Faculty of Physics, Astronomy and Informatics, Nicolaus Copernicus University, 87-100 Torun, Poland;* orcid.org/0000-0003-1560-6315

Lulu Bu − *Univ Lyon, Ens de Lyon, CNRS UMR 5182, Laboratoire de Chimie, F69342 Lyon, France*

Yann Bretonnière − *Univ Lyon, Ens de Lyon, CNRS UMR 5182, Laboratoire de Chimie, F69342 Lyon, France;* orcid.org/0000-0003-1191-6287

Chantal Andraud − *Univ Lyon, Ens de Lyon, CNRS UMR 5182, Laboratoire de Chimie, F69342 Lyon, France*

Ewa Schab-Balcerzak − *Institute of Chemistry, University of Silesia, 40-006 Katowice, Poland; Department of Physical and Theoretical Chemistry, Faculty of Natural Sciences, Comenius University, 84215 Bratislava, Slovakia;* orcid.org/0000-0002-7219-8664

Complete contact information is available at: https://pubs.acs.org/10.1021/acsomega.4c05484

Author Contributions

K.L., investigation, conceptualization, methodology, data curation, formal analysis, verification, visualization, writing−original draft, and writing−review and editing; S.K., investigation, visualization, and writing−review and editing; A.G., conceptualization, resources, methodology, validation, and writing−review and editing; M.S., formal analysis and investigation; K.S., formal analysis and investigation; S.M., resources, validation; L.B., resources; Y.B., conceptualization, resources, and writing−review and editing; C.A., conceptualization, resources, and writing−review and editing; E.S.-B., methodology, validation, writing−review and editing; and L.S., conceptualization, methodology, formal analysis, data curation, visualization, writing−original draft, supervision, funding acquisition, and project administration.

Notes

The authors declare no competing financial interest.

ACKNOWLEDGMENTS

K.L. and L.S. would like to thank the National Science Centre of Poland for financial support within grant no. 2020/39/O/ST5/01865. A.G. thanks the Wroclaw Supercomputer and Networking Center for generous resource allotment. The authors thank Dr. H. Janeczek for the DSC measurements. The authors would like to thank L.B. for the synthesis of the dyes.

ABBREVIATIONS

OLED, organic light-emitting diodes; RL, random laser; RLng, random lasing; OFET, organic field effect transistors; PSC, organic−inorganic hybrid perovskite solar cell; ACQ, aggregation-caused quenching; AIE, aggregation-induced emission; ICT, intramolecular charge transfer; D-π−A, donor-π−acceptor; NIR, near-infrared; TD-DFT, time-dependent density functional theory; SI, Supporting Information; THF, tetrahydrofuran; EED, electron density difference; ΔG, Gibbs free energy; CT, charge transfer; AE, absolute errors; μ_{ES}-μ_{GS}, change in the dipole moment; d_{CT}, charge transfer distance; q_{CT}, total transferred charge; f_w/%, water fraction; $\int I^{emi} d\lambda$, integrated emission spectra; DSC, differential scanning calorimetry; T_m, melting temperature; T_g, glass transition temperature; T_{cc}, crystallization temperature; CV, cyclic voltammetry; DPV, differential pulse voltammetry; IP, ionization potentials; EA, electron affinities; Pt, platinum wire; E_{ox}, first oxidation process; E_{red}, first reduction process;

https://doi.org/10.1021/acsomega.4c05484
ACS Omega 2024, 9, 40769−40782

$E_{red}^{(onset)}$, onset potential of the first reduction process; $E_{ox}^{(onset)}$, onset potential of the first oxidation process; GC, glassy carbon working electrode; PVK, poly(9-vinylcarbazole); PBD, 2-(4-tert-butylphenyl)-5-(4-biphenylyl)-1,3,4-oxadiazole; PMMA, poly(methyl methacrylate); fwhm, full width at half maximum

REFERENCES

(1) Ni, D.; Späth, M.; Klämpfl, F.; Hohmann, M. Properties and Applications of Random Lasers as Emerging Light Sources and Optical Sensors: A Review. *Sensors* **2023**, *23*, No. 247.

(2) Kong, D.; Zhang, K.; Tian, J.; Yin, L.; Sheng, X. Biocompatible and Biodegradable Light-Emitting Materials and Devices. *Adv. Mater. Technol.* **2022**, *7*, No. 2100006.

(3) Benvenuti, E.; Lanfranchi, A.; Moschetto, S.; Natali, M.; Angelini, M.; Lova, P.; et al. On-chip organic optoelectronic system for fluorescence detection. *J. Mater. Chem. C* **2024**, *12*, 4243−4252.

(4) Murawski, C.; Gather, M. C. Emerging Biomedical Applications of Organic Light-Emitting Diodes. *Adv. Opt. Mater.* **2021**, *9*, No. 2100269, DOI: 10.1002/adom.202100269.

(5) Murawski, C.; Pulver, S. R.; Gather, M. C. Segment-specific optogenetic stimulation in Drosophila melanogaster with linear arrays of organic light-emitting diodes. *Nat. Commun.* **2020**, *11*, No. 6248.

(6) Steude, A.; Jahnel, M.; Thomschke, M.; Schober, M.; Gather, M. C. Controlling the Behavior of Single Live Cells with High Density Arrays of Microscopic OLEDs. *Adv. Mater.* **2015**, *27*, 7657−7661.

(7) Jeon, Y.; Choi, H. R.; Park, K. C.; Choi, K. C. Flexible organic light-emitting-diode-based photonic skin for attachable phototherapeutics. *J. Soc. Inf. Disp.* **2020**, *28*, 324−332.

(8) Jeon, Y.; Choi, H. R.; Kwon, J. H.; Choi, S.; Nam, K. M.; Park, K. C.; Choi, K. C. Sandwich-structure transferable free-form OLEDs for wearable and disposable skin wound photomedicine. *Light Sci. Appl.* **2019**, *8*, No. 114, DOI: 10.1038/s41377-019-0221-3.

(9) Krujatz, F.; Hild, O.; Fehse, K.; Jahnel, M.; Werner, A.; Bley, T. Exploiting the Potential of OLED-Based Photo-Organic Sensors for Biotechnological Applications. *Chem. Sci. J.* **2016**, *7*, No. 134, DOI: 10.4172/2150-3494.1000134.

(10) Lochner, C. M.; Khan, Y.; Pierre, A.; Arias, A. C. All-organic optoelectronic sensor for pulse oximetry. *Nat. Commun.* **2014**, *5*, No. 5745.

(11) Bansal, A. K.; Hou, S.; Kulyk, O.; Bowman, E. M.; Samuel, I. D. W. Wearable Organic Optoelectronic Sensors for Medicine. *Adv. Mater.* **2015**, *27*, 7638−7644.

(12) Gayathri, R.; Suchand Sandeep, C. S.; Vijayan, C.; Murukeshan, V. M. Lasing from Micro- and Nano-Scale Photonic Disordered Structures for Biomedical Applications. *Nanomaterials* **2023**, *13*, 2466.

(13) Gomes, A. S. L.; Moura, A. L.; de Araújo, C. B.; Raposo, E. P. Recent advances and applications of random lasers and random fiber lasers. *Prog. Quantum Electron.* **2021**, *78*, 100343.

(14) Shen, H.; Yuan, H.; Bian, Y.; Li, J.; Liu, W.; Xue, H.; Wang, Z. Angular Spectra Tunable Random Lasing for High Contrast Imaging. *Adv. Phys. Res.* **2023**, *2*, No. 2200054.

(15) Santos, E. R.; Takahashi, C. M.; Takimoto, H. G.; Yoshida, S.; Oide, M. T.; Junior, E. C. B.; et al. Low cost spinner developed for deposition of thin films used in OLED devices. *Rev. Bras. Apl. Vacuo* **2018**, *37*, 87.

(16) Gao, L.; Schloemer, T. H.; Zhang, F.; Chen, X.; Xiao, C.; Zhu, K.; Sellinger, A. Carbazole-Based Hole-Transport Materials for High-Efficiency and Stable Perovskite Solar Cells. *ACS Appl. Energy Mater.* **2020**, *3*, 4492−4498.

(17) Xu, X.; Huang, Z.; Liang, X.; Tang, X.; Zhao, Y.; Li, H.; et al. Electronic properties of carbazole/biphenylamino functionalized sulfone-based host materials. *J. Phys. Org. Chem.* **2023**, *36*, No. e4484.

(18) Wex, B.; Kaafarani, B. R. Perspective on carbazole-based organic compounds as emitters and hosts in TADF applications. *J. Mater. Chem. C* **2017**, *5*, 8622−8653.

(19) Karon, K.; Lapkowski, M. Carbazole electrochemistry: a short review. *J. Solid State Electrochem.* **2015**, *19*, 2601−2610.

(20) Lozano-Hernández, L.-A.; Maldonado, J. L.; Garcias-Morales, C.; Espinosa Roa, A.; Barbosa-García, O.; Rodríguez, M.; Pérez-Gutiérrez, E. Efficient OLEDs fabricated by solution process based on carbazole and thienopyrrolediones derivatives. *Molecules* **2018**, *23*, No. 280.

(21) Arai, A.; Sasabe, H.; Nakao, K.; Masuda, Y.; Kido, J. π-Extended Carbazole Derivatives as Host Materials for Highly Efficient and Long-Life Green Phosphorescent Organic Light-Emitting Diodes. *Chem. - Eur. J.* **2021**, *27*, 4971−4976.

(22) Ledwon, P. Recent advances of donor-acceptor type carbazole-based molecules for light emitting applications. *Org. Electron.* **2019**, *75*, No. 105422.

(23) Boudreault, P. L. T.; Virkar, A. A.; Bao, Z.; Leclerc, M. Synthesis and characterization of soluble indolo[3,2-b]carbazole derivatives for organic field-effect transistors. *Org. Electron.* **2010**, *11*, 1649−1659.

(24) Souharce, B.; Kudla, C. J.; Forster, M.; Steiger, J.; Anselmann, R.; Thiem, H.; Scherf, U. Amorphous carbazole-based (Co)polymers for OFET application. *Macromol. Rapid Commun.* **2009**, *30*, 1258−1262.

(25) Jegorovė, A.; Truong, M. A.; Murdey, R.; Daskeviciene, M.; Malinauskas, T.; Kantminiene, K.; et al. Starburst Carbazole Derivatives as Efficient Hole Transporting Materials for Perovskite Solar Cells. *Sol. RRL* **2022**, *6*, No. 2100877.

(26) Kotowicz, S.; Korzec, M.; Małecki, J. G.; Pająk, A. K.; Łuczak, A.; Jung, J.; et al. Carbazole core derivatives and their photophysical and electrochemical investigations supported by the theoretical calculations. *Synth. Met.* **2024**, *301*, No. 117533.

(27) Cataldo, S.; Pignataro, B. Polymeric thin films for organic electronics: Properties and adaptive structures. *Materials* **2013**, *6* (3), 1159−1190, DOI: 10.3390/ma6031159.

(28) Ansari, S. P.; Ali, F. Conjugated Organic Polymers for Optoelectronic Devices. In *Functional Polymers. Polymers and Polymeric Composites: A Reference Series*; Jafar Mazumder, M.; Sheardown, H.; Al-Ahmed, A., Eds.; Springer: Cham, 2018; p 1.

(29) Ngai, J. H. L.; Ho, J. K. W.; Chan, R. K. H.; Cheung, S. H.; Leung, L. M.; So, S. K. Growth, characterization, and thin film transistor application of CH3NH3PbI3 perovskite on polymeric gate dielectric layers. *RSC Adv.* **2017**, *7*, 49353−49360.

(30) Sznitko, L.; Mysliwiec, J.; Miniewicz, A. The role of polymers in random lasing. *J. Polym. Sci., Part B: Polym. Phys.* **2015**, *53*, 951−974.

(31) Ma, X.; Sun, R.; Cheng, J.; Liu, J.; Gou, F.; Xiang, H.; Zhou, X. Fluorescence Aggregation-Caused Quenching versus Aggregation-Induced Emission: A Visual Teaching Technology for Undergraduate Chemistry Students. *J. Chem. Educ.* **2016**, *93*, 345−350.

(32) da Costa, R. G. M.; dos Santos Carvalho, R.; Isoppo, V. G.; Barreto, A. R. J.; Peñafiel, M. J. P.; dos Santos, A. M.; et al. Aryloxy-benzothiadiazole-chalcone and aryloxy-benzothiadiazole-fluorene AIEE luminogens: Synthesis, photophysical properties, and electroluminescence evaluation. *Dyes Pigm.* **2023**, *219*, 111533.

(33) Filipek, P.; Karoń, K.; Hellwig, H.; Szłapa-Kula, A.; Filapek, M. The Role of Intermolecular Interaction on Aggregation-Induced Emission Phenomenon and OLED Performance. *Materials* **2022**, *15*, 8525.

(34) Yu, M.; Huang, R.; Guo, J.; Zhao, Z.; Tang, B. Z. Promising applications of aggregation-induced emission luminogens in organic optoelectronic devices. *PhotoniX* **2020**, *1*, No. 11.

(35) Lupinska, K.; Durko, M.; Andraud, C.; Bretonnière, Y.; Hanczyc, P.; Fita, P.; et al. One- and two-photon lasing from TCF-based AIE dye. *J. Mater. Chem. C* **2023**, *11*, 4937−4945, DOI: 10.1039/d2tc04673c.

(36) Ignesti, E.; Tommasi, F.; Fini, L.; Martelli, F.; Azzali, N.; Cavalieri, S. A new class of optical sensors: A random laser based device. *Sci. Rep.* **2016**, *6*, No. 35225.

(37) Padiyakkuth, N.; Thomas, S.; Antoine, R.; Kalarikkal, N. Recent progress and prospects of random lasers using advanced materials. *Mater. Adv.* **2022**, *3*, 6687−6706.

https://doi.org/10.1021/acsomega.4c05484
ACS Omega 2024, 9, 40769−40782

(38) Hou, Y.; Zhou, Z.; Zhang, C.; Tang, J.; Fan, Y.; Xu, F. F.; Zhao, Y. S. Full-color flexible laser displays based on random laser arrays. *Sci. China Mater.* **2021**, *64*, 2805−2812.
(39) Padiyakkuth, N.; Antoine, R.; Kalarikkal, N. Electrospun polyvinylidene fluoride mats as a novel platform for dye-doped random lasing. *J. Lumin.* **2022**, *252*, No. 119296.
(40) Wang, Y.; Duan, Z.; Qiu, Z.; Zhang, P.; Wu, J.; Zhang, D.; Dingke, A. Random lasing in human tissues embedded with organic dyes for cancer diagnosis. *Sci. Rep.* **2017**, *7*, No. 8385.
(41) Misra, R.; Bhattacharyya, S. P. *Intramolecular Charge Transfer: Theory and Applications*, 2018.
(42) Indig, G. L. Mechanism of dye bleaching upon laser excitation of crystal violet bound to bovine serum albumin. *Chem. Lett.* **1997**, *26*, 243−244.
(43) Bureš, F. Fundamental aspects of property tuning in push-pull molecules. *RSC Adv.* **2014**, *4*, 58826−58851.
(44) Jin, R.; Zhang, X.; Xiao, W. Theoretical studies of photophysical properties of d−π−a−π−D-type diketopyrrolopyrrole-based molecules for organic light-emitting diodes and organic solar cells. *Molecules* **2020**, *25*, 667.
(45) Oligomers, D.; Sharbati, M. T.; Panahi, F.; Gharavi, A. Near-Infrared Organic Light-Emitting Diodes Based on donor-pi-acceptor oligomers. *IEEE Photonics Technol. Lett.* **2010**, *22*, 1695−1697, DOI: 10.1109/LPT.2010.2081358.
(46) Shi, X.; Bian, Y.; Tong, J.; Liu, D.; Zhou, J.; Wang, Z. Chromaticity-tunable white random lasing based on a microfluidic channel. *Opt. Express* **2020**, *28*, 13576.
(47) Kedia, S.; Sinha, S. Random laser emission at dual wavelengths in a donor-acceptor dye mixture solution. *Results Phys.* **2017**, *7*, 697−704.
(48) Rémond, M.; Zheng, Z.; Jeanneau, E.; Andraud, C.; Bretonnière, Y.; Redon, S. 4,5,5-Trimethyl-2,5-dihydrofuran-Based Electron-Withdrawing Groups for NIR-Emitting Push-Pull Dipolar Fluorophores. *J. Org. Chem.* **2019**, *84*, 9965−9974.
(49) Frisch, M. J.; Trucks, G. W.; Schlegel, H. B.; Scuseria, G. E.; Robb, M. A.; Cheeseman, J. R.; Scalmani, G.; Barone, V.; Petersson, G. A.; Nakatsuji, H.; Li, X.; Caricato, M.; Marenich, A. V.; Bloino, J.; Janesko, B. G.; Gomperts, R.; Mennucci, B.; Hratchian, H. P.; Ortiz, J. V.; Izmaylov, A. F.; Sonnenberg, J. L.; Williams-Young, D.; Ding, F.; Lipparini, F.; Egidi, F.; Goings, J.; Peng, B.; Petrone, A.; Henderson, T.; Ranasinghe, D.; Zakrzewski, V. G.; Gao, J.; Rega, N.; Zheng, G.; Liang, W.; Hada, M.; Ehara, M.; Toyota, K.; Fukuda, R.; Hasegawa, J.; Ishida, M.; Nakajima, T.; Honda, Y.; Kitao, O.; Nakai, H.; Vreven, T.; Throssell, K.; Montgomery, J. A., Jr.; Peralta, J. E.; Ogliaro, F.; Bearpark, M. J.; Heyd, J. J.; Brothers, E. N.; Kudin, K. N.; Staroverov, V. N.; Keith, T. A.; Kobayashi, R.; Normand, J.; Raghavachari, K.; Rendell, A. P.; Burant, J. C.; Iyengar, S. S.; Tomasi, J.; Cossi, M.; Millam, J. M; Klene, M.; Adamo, C.; Cammi, R.; Ochterski, J. W.; Martin, R. L.; Morokuma, K.; Farkas, O.; Foresman, J. B.; Fox, D. J. *Gaussian 16*, Revision C.01, Gaussian, Inc., Wallingford CT, 2016.https://gaussian.com/citation/ n.d.
(50) Yu, H. S.; He, X.; Li, S. L.; Truhlar, D. G. MN15: A Kohn-Sham global-hybrid exchange-correlation density functional with broad accuracy for multi-reference and single-reference systems and noncovalent interactions. *Chem. Sci.* **2016**, *7*, 5032−5051.
(51) Grabarz, A. M.; Ośmiałowski, B. Benchmarking density functional approximations for excited-state properties of fluorescent dyes. *Molecules* **2021**, *26*, No. 7434.
(52) Tomasi, J.; Mennucci, B.; Cammi, R. Quantum mechanical continuum solvation models. *Chem. Rev.* **2005**, *105*, 2999−3093.
(53) Miertuš, S.; Scrocco, E.; Tomasi, J. Electrostatic interaction of a solute with a continuum. A direct utilizaion of AB initio molecular potentials for the prevision of solvent effects. *Chem. Phys.* **1981**, *55*, 117−129.
(54) Cammi, R.; Mennucci, B. Linear response theory for the polarizable continuum model. *J. Chem. Phys.* **1999**, *110*, 9877−9886.
(55) Cossi, M.; Barone, V. Time-dependent density functional theory for molecules in liquid solutions. *J. Chem. Phys.* **2001**, *115*, 4708−4717.
(56) Caricato, M.; Mennucci, B.; Tomasi, J.; Ingrosso, F.; Cammi, R.; Corni, S.; Scalmani, G. Formation and relaxation of excited states in solution: A new time dependent polarizable continuum model based on time dependent density functional theory. *J. Chem. Phys.* **2006**, *124*, No. 124520, DOI: 10.1063/1.2183309.
(57) Le Bahers, T.; Adamo, C.; Ciofini, I. A Qualitative Index of Spatial Extent in Charge-Transfer Excitations. *J. Chem. Theory Comput.* **2011**, *7*, 2498−2506.
(58) Bujak, P.; Kulszewicz-Bajer, I.; Zagorska, M.; Maurel, V.; Wielgus, I.; Pron, A. Polymers for electronics and spintronics. *Chem. Soc. Rev.* **2013**, *42*, 8895−8999.
(59) Ipuy, M.; Liao, Y. Y.; Jeanneau, E.; Baldeck, P. L.; Bretonnière, Y.; Andraud, C. Solid state red biphotonic excited emission from small dipolar fluorophores. *J. Mater. Chem. C* **2016**, *4*, 766−779.
(60) Redon, S.; Eucat, G.; Ipuy, M.; Jeanneau, E.; Gautier-Luneau, I.; Ibanez, A.; et al. Tuning the solid-state emission of small push-pull dipolar dyes to the far-red through variation of the electron-acceptor group. *Dyes Pigm.* **2018**, *156*, 116−132.
(61) Chiu, S. K.; Chung, Y. C.; Liou, G. S.; Su, Y. O. Electrochemical and spectral characterizations of 9-phenylcarbazoles. *J. Chin. Chem. Soc.* **2012**, *59*, 331−337.
(62) Hsiao, S. H.; Lin, S. W. Electrochemical synthesis of electrochromic polycarbazole films from N-phenyl-3,6-bis(N-carbazolyl)carbazoles. *Polym. Chem.* **2016**, *7*, 198−211.
(63) Lu, L.; Guo, Y.; Zhao, B.; Wang, H.; Miao, Y. A new strategy to develop simple and efficient monochrome and white organic light-emitting diodes. *Mater. Today* **2024**, *74*, 109−120.
(64) Miao, Y.; Wang, G.; Yin, M.; Guo, Y.; Zhao, B.; Wang, H. Phosphorescent ultrathin emitting layers sensitized by TADF interfacial exciplex enables simple and efficient monochrome/white organic light-emitting diodes. *Chem. Eng. J.* **2023**, *461*, 141921.
(65) Du, M.; Yang, Z.; Miao, Y.; Wang, C.; Dong, P.; Wang, H.; Guo, K. Facile Nanowelding Process for Silver Nanowire Electrodes Toward High-Performance Large-Area Flexible Organic Light-Emitting Diodes. *Adv. Funct Mater.* **2024**, No. 2404567, DOI: 10.1002/adfm.202404567.
(66) Szukalska, A.; Zajac, D.; Cyprych, K.; Mysliwiec, J. Ultra-Photostable Random Lasing Coming from the Benzothiadiazole Derivative Dye-Doped Organic System. *J. Phys. Chem. C* **2023**, *127*, 24618−24625.
(67) Redding, B.; Choma, M. A.; Cao, H. Spatial coherence of random laser emission. *Opt. Lett.* **2011**, *36*, 3404−3406.
(68) Paschotta, R.Gaussian Pulses. In *RP Photonics Encyclopedia*, 2023.
(69) Wang, H.; Li, Q.; Alam, P.; Bai, H.; Bhalla, V.; Bryce, M. R.; et al. Aggregation-Induced Emission (AIE), Life and Health. *ACS Nano* **2023**, *17*, 14347−14405.
(70) Yambem, S. D.; Brooks-Richards, T. L.; Forrestal, D. P.; Kielar, M.; Sah, P.; Pandey, A. K.; Woodruff, M. A. Spectral changes associated with transmission of OLED emission through human skin. *Sci. Rep.* **2019**, *9*, No. 9875.
(71) Choi, S.; Na, Y.; Lee, J.; Choi, K. C. 41.1: *Invited Paper:* [Invited] Textile-Oleds With High Wearing Comfort Used for Fashion Displays and Phototherapy Applications. In *SID Symposium Digest of Technical Papers*, 2021; Vol. 52, p 279.
(72) Lee, S.-Y. Colloidal Optics and Photonics: Photonic Crystals, Plasmonics, and Metamaterials. *Curr. Opt. Photonics* **2017**, *1* (6), 239−246, DOI: 10.3807/COPP.2023.7.6.608.
(73) Wei, G. Q.; Tao, Y. C.; Wu, J. J.; Li, Z. Z.; Zhuo, M. P.; Wang, X. D.; Liao, L. S. Low-Threshold Organic Lasers Based on Single-Crystalline Microribbons of Aggregation-Induced Emission Luminogens. *J. Phys. Chem. Lett.* **2019**, *10*, 679−684.
(74) Wang, Z.; Kapsalidis, F.; Wang, R.; Beck, M.; Faist, J. Ultra-low threshold lasing through phase front engineering via a metallic circular aperture. *Nat. Commun.* **2022**, *13*, No. 230.
(75) Chen, V. W.; Sobeshchuk, N.; Lafargue, C.; Mansfield, E. S.; Yom, J.; Johnstone, L. R.; et al. Three-dimensional organic microlasers with low lasing thresholds fabricated by multiphoton and UV lithography. *Opt. Express* **2014**, *22*, 12316.

(76) Yoshida, K.; Gong, J.; Kanibolotsky, A. L.; Skabara, P. J.; Turnbull, G. A.; Samuel, I. D. W. Electrically driven organic laser using integrated OLED pumping. *Nature* **2023**, *621*, 746−752.
(77) Ash, C.; Dubec, M.; Donne, K.; Bashford, T. Effect of wavelength and beam width on penetration in light-tissue interaction using computational methods. *Lasers Med. Sci.* **2017**, *32*, 1909−1918.
(78) Melendez-Celis, U.; Spezzia-Mazzocco, T.; Persheyev, S.; Lian, C.; Samuel, I.; Ramirez-San-Juan, J. C.; Ramos-Garcia, R. Organic light emitting diode for in vitro antimicrobial photodynamic therapy of Candida strains. *Photodiagn. Photodyn. Ther.* **2021**, *36*, No. 102567.
(79) Piksa, M.; Lian, C.; Samuel, I. C.; Pawlik, K. J.; Samuel, I. D. W.; Matczyszyn, K. The role of the light source in antimicrobial photodynamic therapy. *Chem. Soc. Rev.* **2023**, *52*, 1697−1722.
(80) Gayathri, R.; Suchand Sandeep, C. S.; Vijayan, C.; Murukeshan, V. M. Random Lasing for Bimodal Imaging and Detection of Tumor. *Biosensors* **2023**, *13*, No. 1003.

https://doi.org/10.1021/acsomega.4c05484
ACS Omega 2024, 9, 40769−40782